

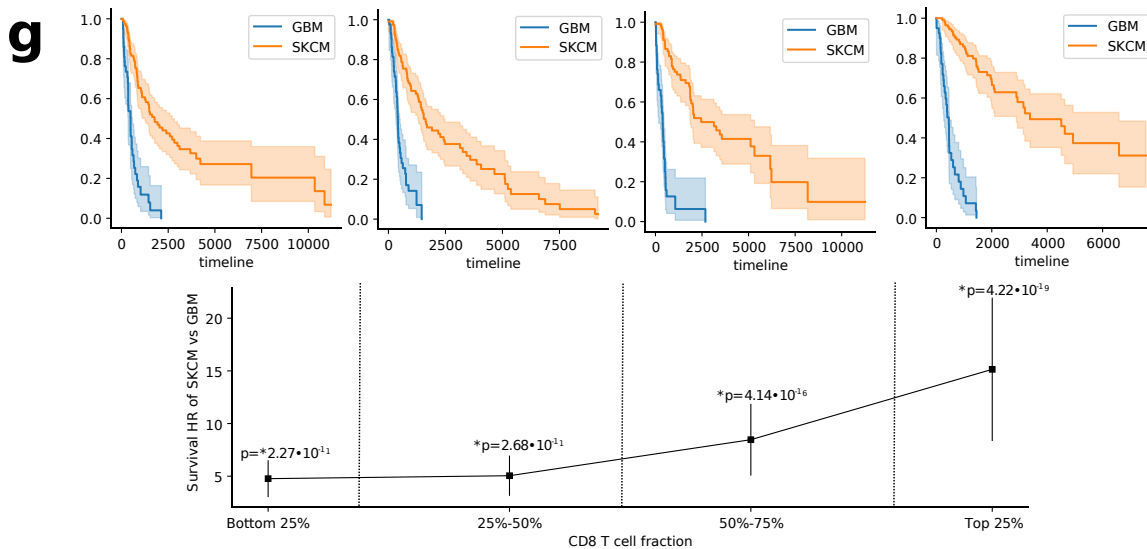
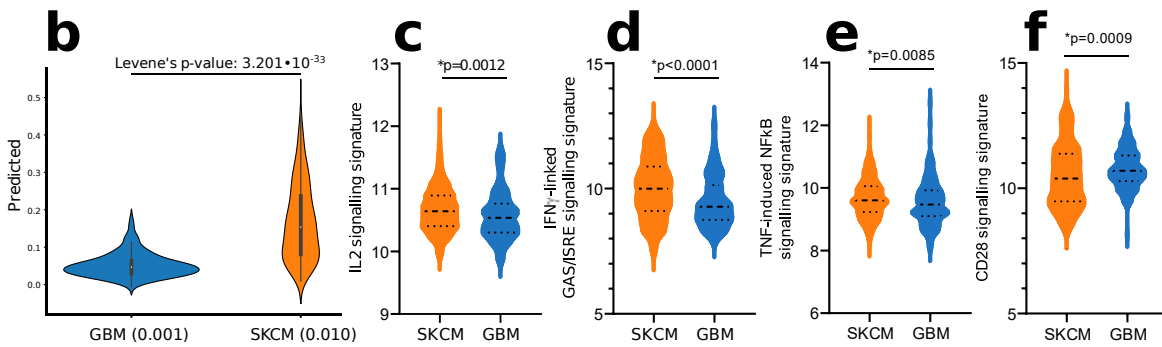
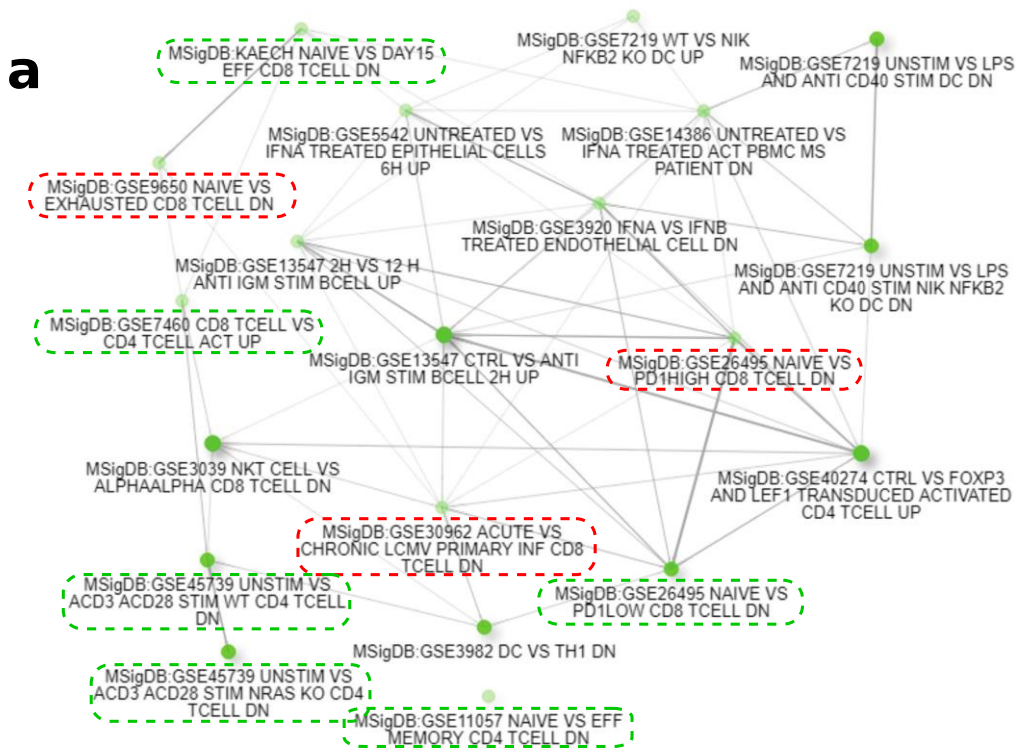
SUPPLEMENTARY FIGURES

Immunogenomic, single-cell and spatial dissection of CD8⁺T cell exhaustion reveals critical determinants of cancer immunotherapy

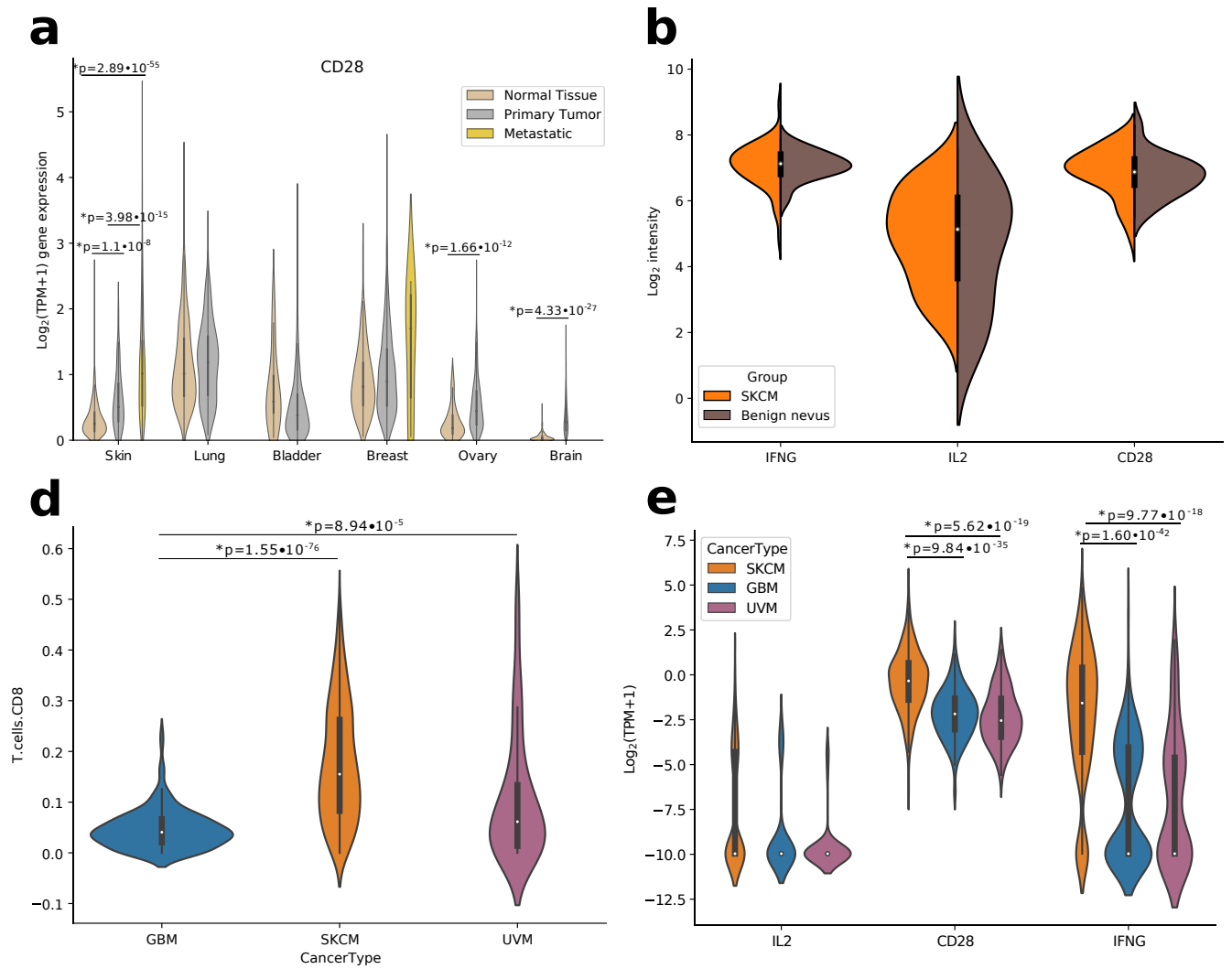
Stefan Naulaerts,^{1,2,23} Daniel M Borrás,^{3,23} Asier Antoranz Martínez,^{4,23} Julie Messiaen,⁴ Yannick Van Herck,⁵ Lendert Gelens,⁶ Tom Venken,^{7,8} Isaure Vanmeerbeek,³ Sanket More,⁹ Jenny Sprooten,³ Oliver Bechter,⁵ Gabriele Bergers,^{10,11} Adrian Liston,^{12,13,14} Steven De Vleeschouwer,^{15,16,17} Benoit J Van Den Eynde,^{1,2} Diether Lambrechts,^{7,8} Jannie Borst,¹⁸ Francesca Bosisio,^{19,21} Sabine Tejpar,^{20,21} Frederik De Smet,^{4,21} Abhishek D Garg,^{3,21,*}

¹Ludwig Institute for Cancer Research, Brussels, Belgium; ²De Duve Institute, UC Louvain, Brussels, Belgium; ³Laboratory of Cell Stress & Immunity, Department of Cellular & Molecular Medicine, KU Leuven, Belgium; ⁴Laboratory for Precision Cancer Medicine, Translational Cell and Tissue Research, Department of Imaging & Pathology, KU Leuven, Belgium; ⁵Laboratory of Experimental Oncology, Department of Oncology, KU Leuven, Belgium; Department of General Medical Oncology, UZ Leuven, Belgium; ⁶Laboratory of Dynamics in Biological Systems, Department of Cellular & Molecular Medicine, KU Leuven, Belgium; ⁷Laboratory of Translational Genetics, Department of Human Genetics, KU Leuven, Belgium; ⁸VIB Center for Cancer Biology, VIB, Leuven, Belgium; ⁹Laboratory of Cell Death Research & Therapy, Department of Cellular & Molecular Medicine, KU Leuven, Belgium; ¹⁰Laboratory of Tumor Microenvironment and Therapeutic Resistance, Department of Oncology, VIB-Center for Cancer Biology, KU Leuven, Leuven, Belgium; ¹¹Department of Neurological Surgery, UCSF Comprehensive Cancer Center, UCSF, San Francisco, CA, United States; ¹²VIB Center for Brain and Disease Research, Leuven, Belgium; ¹³Department of Microbiology and Immunology, KU Leuven, Belgium; ¹⁴Laboratory of Lymphocyte Signalling and Development, The Babraham Institute, Cambridge, UK; ¹⁵Department of Neurosurgery, University Hospitals Leuven, Leuven, Belgium; ¹⁶Laboratory of Experimental Neurosurgery and Neuroanatomy, Department of Neurosciences, KU Leuven, Belgium; ¹⁷Leuven Brain Institute (LBI), Leuven, Belgium; ¹⁸Department of Immunology and OncoCode Institute, Leiden University Medical Center, Leiden, Netherlands; ¹⁹Translational Cell & Tissue Research, Department of Imaging & Pathology, KU Leuven, Belgium; ²⁰Laboratory for Molecular Digestive Oncology, Department of Oncology, KU Leuven, Belgium; ²¹These authors had equal contributions;

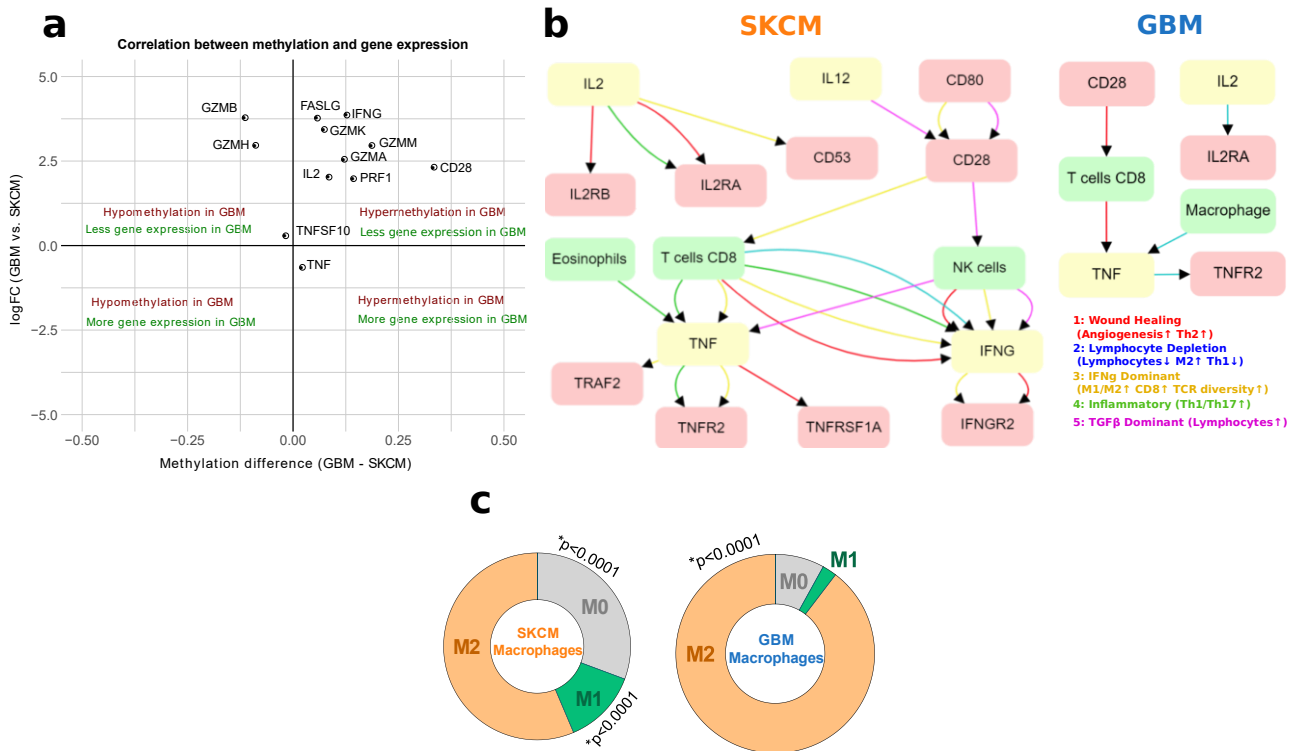
*Correspondence: abhishek.garg@kuleuven.be



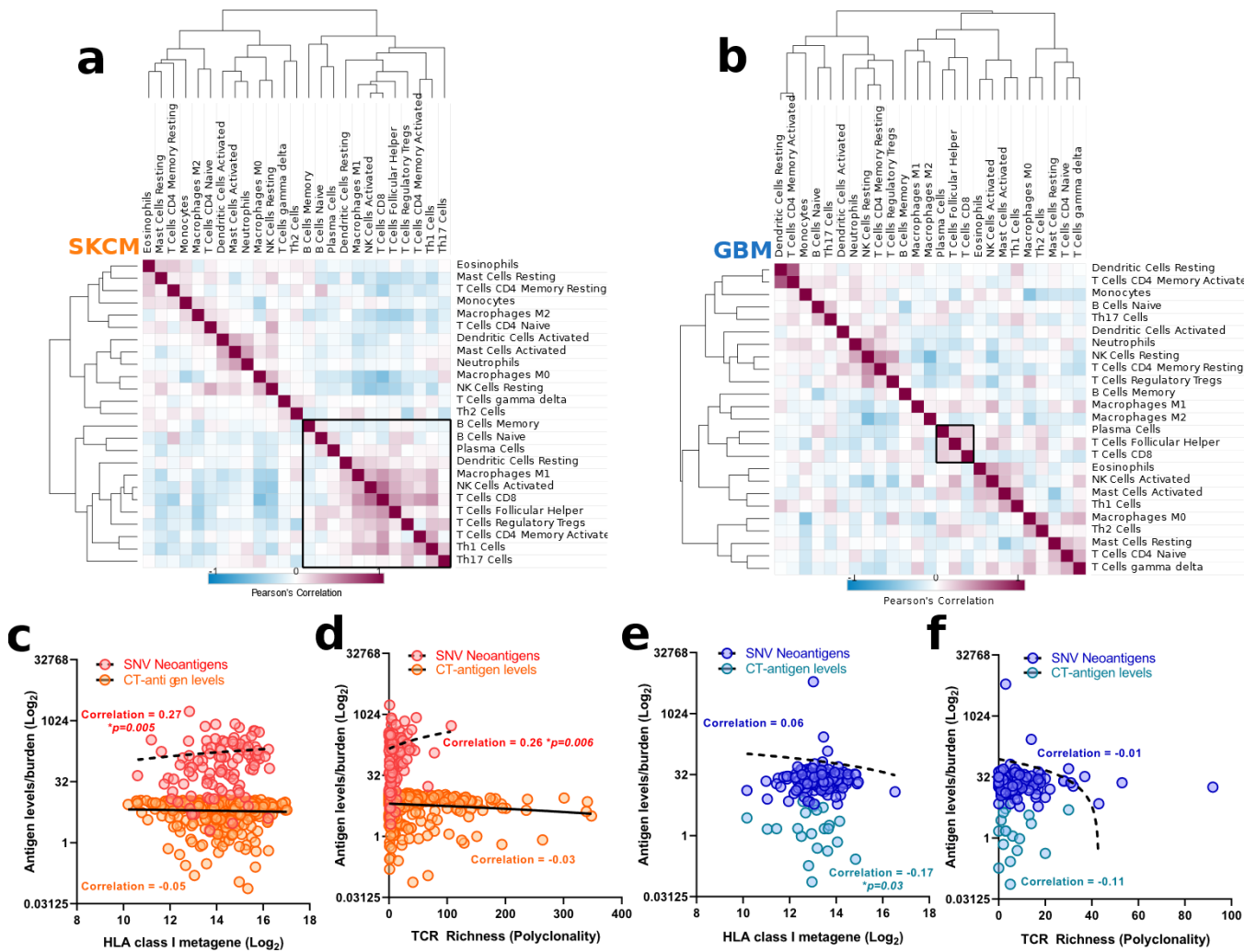
Supplementary Figure SI. (a) A network depicting top 20 human Immune-MSigDB datasets enriched by the $CD8^+$ T cell-signature. The nodes connect the different datasets if $\geq 20\%$ genes are shared between them. Darker nodes are more significantly enriched (FDR adjusted p -value <0.05), bigger nodes represent datasets with higher number of genes and thicker edges indicate higher overlapping genes. Green rectangles indicate effector/memory lymphocytes-related datasets and red rectangles indicate lymphocyte exhaustion-related datasets. **(b)** Distribution of AI/ML-model predicted values in TCGA-GBM and TCGA-SKCM datasets. The variance (between brackets) in GBM predictions is ten times less than in SKCM. This difference is statistically highly significant (Levene's test). These results connect to the plot in **Figure Ig**, wherein LOOCV performance indicates that the GBM-specific model is worse at predicting the trend (Pearson correlation between $CD8^+$ T-cell signature vs. $CD8^+$ T cell-fractions predictions) in TCGA-GBM samples than the corresponding SKCM-specific model in TCGA-SKCM samples, exemplified by the substantially lower-variability in GBM-model. This is because, the low variance in GBM predictions as compared to SKCM means that the GBM-model is performing worse than SKCM; because an AI/ML-model that is successfully "learning" and generating reliable predictions tends to have higher variance owing to the natural variations of a dynamic patient population (e.g., SKCM) while lack of any meaningful predictions will lead to a minimally variable output (e.g., GBM). Feature weights also do not transfer well between both cancer types (**Figure Ig**, green-line). There is a statistically significant difference in mean prediction error (Welch t-test, p -value= 7.14×10^{-5}), however, the effect size of this is small (Cohen's D, 0.310). The GBM model does not underfit the training data (training set $R_p=0.99$) and is responsive to changes in input features (test set $R_p=0.03$ using scrambled features). **(c-f)** Violin-plot of indicated signature's expression levels in TCGA-GBM and TCGA-SKCM datasets (Mann-Whitney test). **(g)** Analyses of $CD8^+$ T cell-fractions' quadrant analysis: all quartiles were split off, based on the $CD8^+$ T cell-fraction values arranged from lowest to highest 25% patient subgroups, inferred by CIBERSORT per cancer-type, individually. Per quartile, the Kaplan-Meier curves were plotted. The multi-variate CoxPh hazard ratios for GBM vs SKCM were estimated for each quartile of $CD8^+$ T cell-fraction values. Features were z-score standardized. Statistical-significance threshold was $*p<0.05$. For different gene-signatures, see **Supplementary-Table.2**.



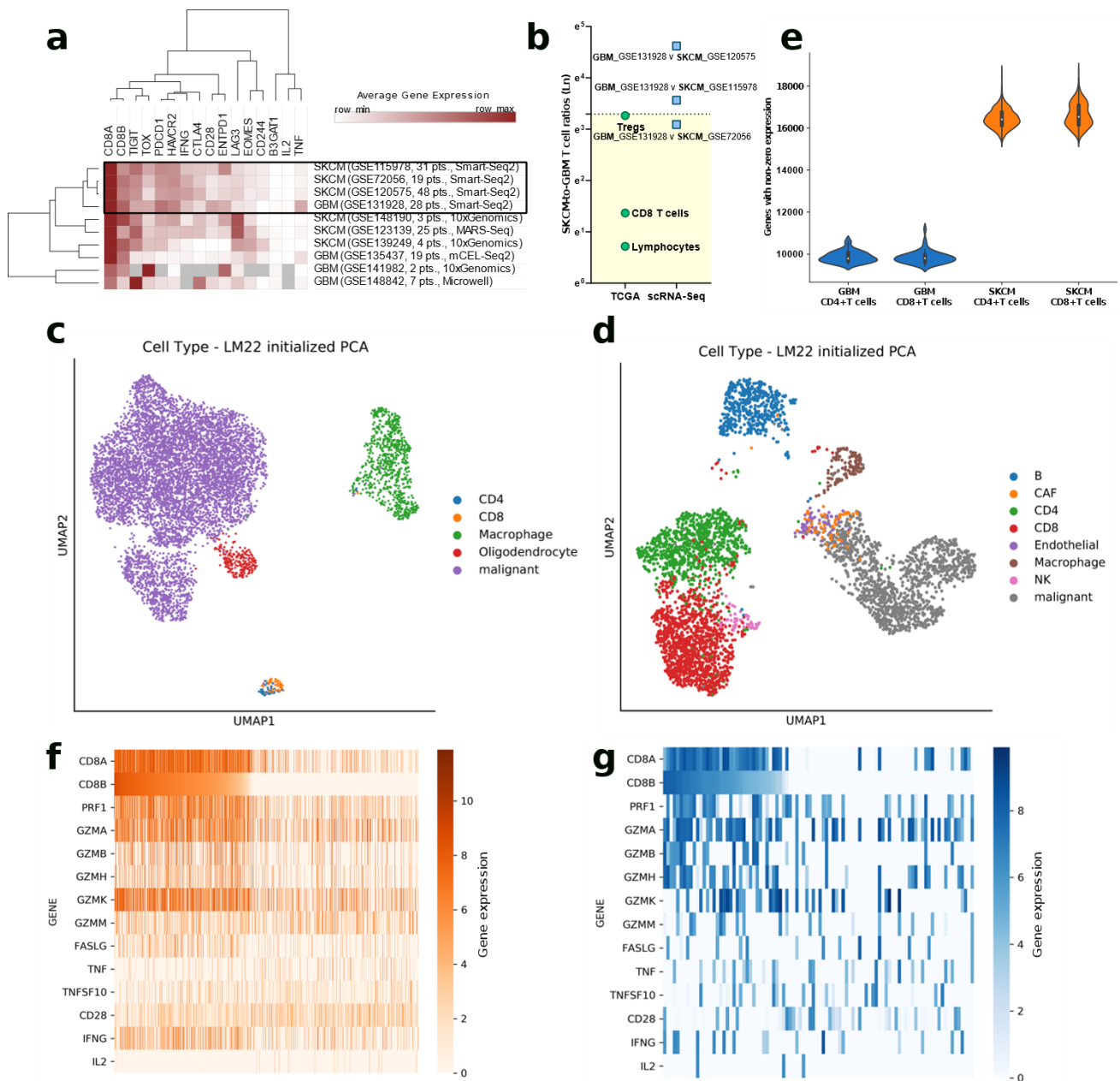
Supplementary Figure S2. (a) Violin-plots comparing CD28 expression between TCGA primary-tumour/metastasis bulk-RNAseq vs. Genotype-Tissue Expression (GTEx) normal-organ/tissue bulk-RNAseq datasets (Welch's t-test). Brain (normal-tissue, n=207; primary-tumour, n=153), bladder (normal-tissue, n=9; primary-tumour, n=407), breast (normal-tissue, n=179; primary-tumour, n=1092; metastatic-tissue, n=7), lung (normal-tissue, n=288; primary-tumour, n=513), ovary (normal-tissue, n=88; primary-tumour, n=419), skin (normal-tissue, n=557; primary-tumour, n=102; metastatic-tissue, n=366). **(b)** Violin-plots comparing expression of indicated genes between primary-melanoma (n=45) and benign nevi (n=18). Violin-plots comparing CD8⁺T cell-fractions **(c)**, IFNG-IL2-CD28 **(d)** expressions between TCGA SKCM (n=470), GBM (n=171) and UVM (n=79) bulk-RNAseq datasets (Welch's t-test). Statistical-significance threshold was * $p < 0.05$. For different gene-signatures, see **Supplementary-Table.2**.



Supplementary Figure S3. (a) Scatterplot illustrating the relation between DNA methylation and gene-expression patterns for the indicated genes within TCGA-SKCM/GBM datasets. The X-axis shows the shift in methylation β -value, while the Y-axis represents the expression-ratio between GBM and SKCM patients. **(b)** Extracellular network-analyses¹ driven by interaction between CD8⁺T cell-fractions and *IFNG-IL2-CD28-TNF* depicting interactions between other “recruited” extracellular signalling ligands/cytokines and CIBERSORT-LM22 immune-deconvoluted immune cell fractions¹ within TCGA-SKCM or TCGA-GBM patient-datasets. Herein, the nodes indicate receptors, ligands or cell-types whereas the edges indicate specific enrichment of tumour immune-landscape features across specific patient subsets. Overall, these analyses indicate subset of patients enriching for particular tumour immune-landscape pathway and embedment of particular ligand-receptor-cell interactions within that landscape in those patient-subsets.¹ **(c)** Doughnut-plots representing average CIBERSORT-LM22 M0, M1 or M2 macrophage-fractions¹ in TCGA-SKCM or TCGA-GBM. Statistical estimate was done for SKCM vs. GBM comparison (Kruskal-Wallis ANOVA test with Dunn’s multiple comparisons test). Statistical-significance threshold was *p < 0.05. For different gene-signatures, see **Supplementary-Table.2.**

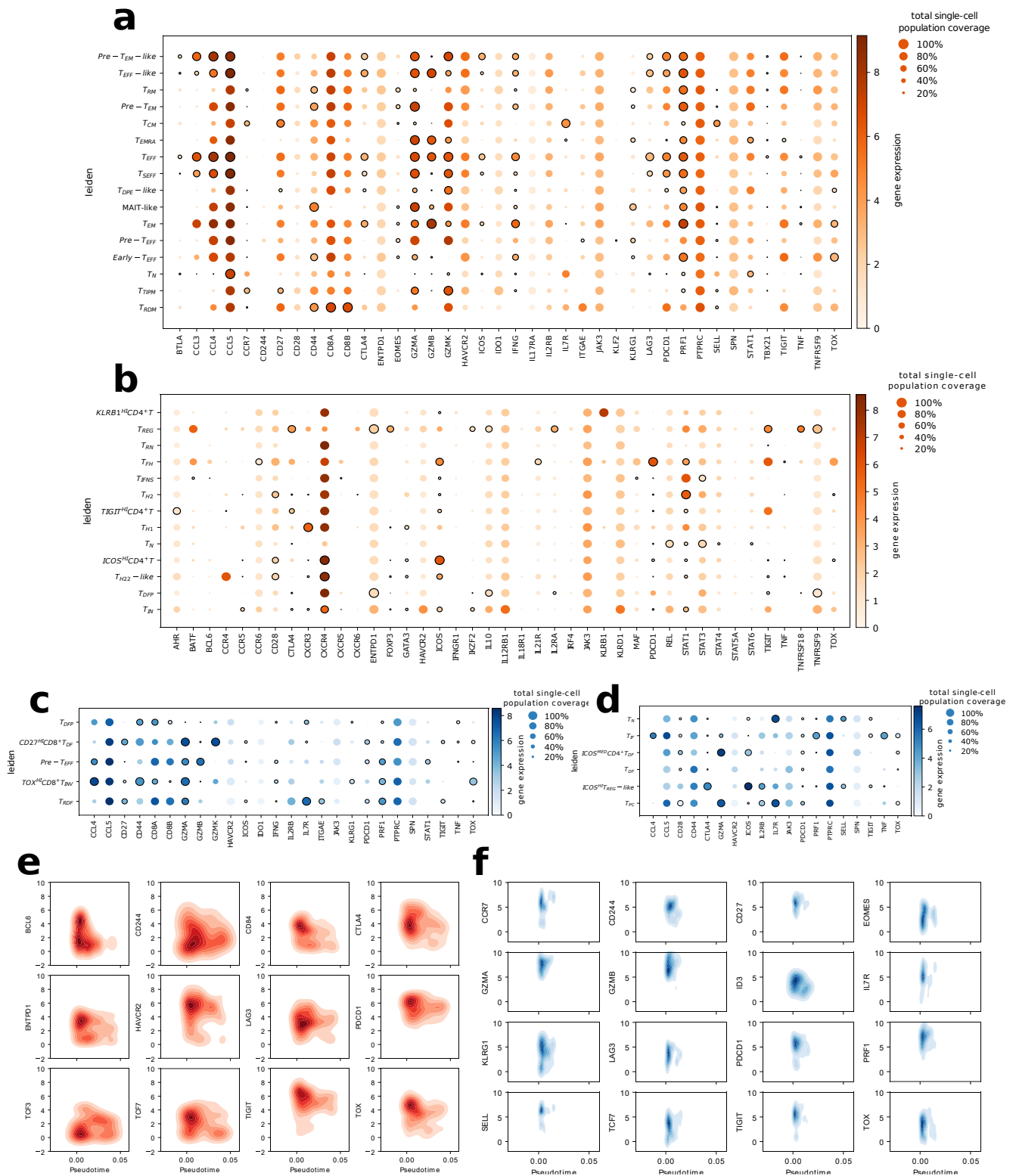


Supplementary Figure S4. (a,b) Correlation-matrices for different CIBERSORT-LM22 or CRI iATLAS based immune-deconvolution derived immune-cell fractions¹ across all TCGA-SKCM (a) or TCGA-GBM (b) patients. Spearman's correlation between indicated antigen-burdens (i.e., SNV-neoantigens or CT-antigen signature) and HLA class-I signature (c,e) or T-cell receptor (TCR) Richness (d,f) across TCGA-SKCM (c,d) or TCGA-GBM (e,f) patients. Statistical-significance threshold was * $p < 0.05$. For different gene-signatures, see **Supplementary-Table.2**.



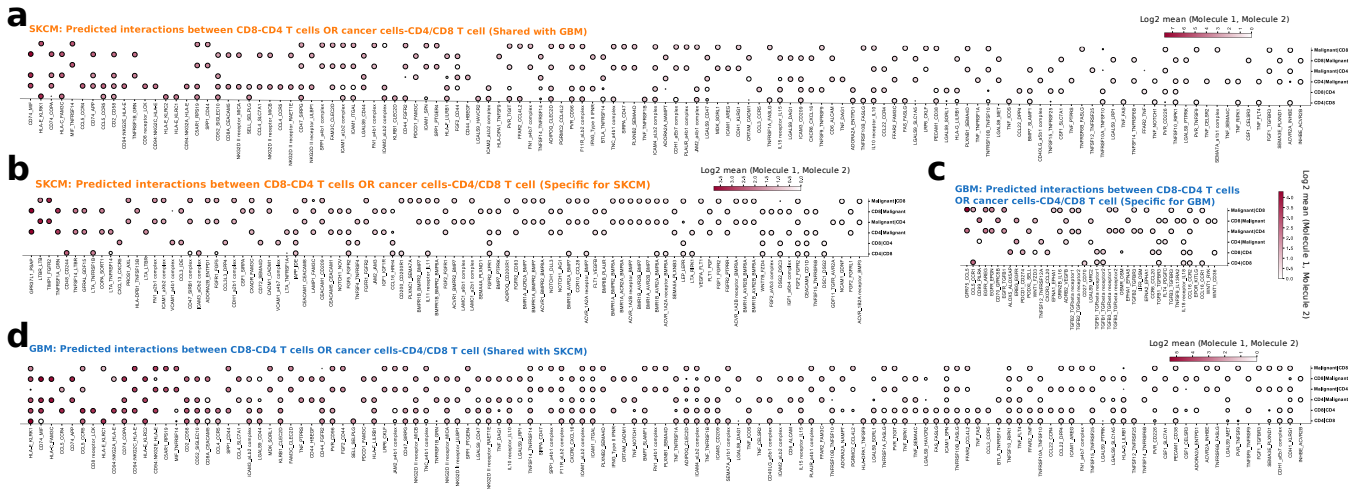
Supplementary Figure S5. (a) Results of a literature-wide meta-analysis for previously published single-cell (sc)RNASeq maps profiling SKCM or GBM patient-derived tumours for immune cell-compartment, especially T cells. This analysis was conducted via the Tumor Immune Single Cell Hub (TISCH) database,² a large-scale curated database integrating single-cell transcriptomics data from >2 million cells across at least 76 high-quality tumour-datasets from 28 cancer-types.² Heatmap indicates the coverage of csCD8⁺T cell-signature (average gene-expression) within CD8⁺T cells' single-cell transcriptomics data across all the scRNASeq-datasets. The black-outlined box indicates the scRNASeq-datasets with the best gene-by-gene coverage for csCD8⁺T cell-signature across SKCM or GBM patient-cohorts. Grey box indicates lack of expression or gene "drop-outs". (b) SKCM-to-GBM ratios for indicated CIBERSORT-LM22/CRI-iATLAS derived immune-cell fractions within TCGA-datasets (green circles) or number of total T cells profiled across major scRNASeq datasets (blue squares) previously delineated (Figure S5a). (c,d) UMAP-visualizations of indicated immune cell-types, based on CIBERSORT-LM22 gene-signatures, in GBM (c) or SKCM (d) scRNASeq patient-cohorts.^{3,4} Herein, for SKCM, scRNASeq profiling was done in 19-patients to derive 1252 melanoma-cells, 61 cancer-associated fibroblasts (CAFs), 2069 T-cells, 515 B-cells, 52 NK-cells, 126 macrophages and 65 endothelial cells.³ For this profiling, the SKCM-tumour tissue originated from primary-melanoma (n=1) or metastasis procured

from lymphoid tissue (n=9 from lymph-nodes, n=1 from spleen), subcutaneous/intramuscular tissue (n=5) or gastrointestinal tract (n=3).³ Similarly, for GBM, scRNASeq profiling was done in 28-patients to derive 6863 GBM-cancer cells, 219 oligodendrocytes, 754 macrophages and 94 T-cells.⁴ For this profiling, the GBM-tumour tissue originated from IDH-wild-type adult (n=20) and paediatric (n=8) GBM-patients.⁴ **(e)** Visualization of gene-dropout. The number of genes with non-zero expression are shown for GBM and SKCM associated CD4⁺/CD8⁺ T single-cells. **(f,g)** Heatmap representation of indicated gene's expression levels across single T-cells (sorted by *CD8B*) within the SKCM **(f)** or GBM **(g)** scRNAseq patient-datasets.

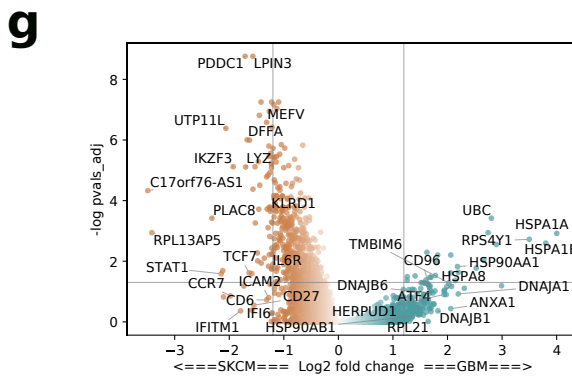
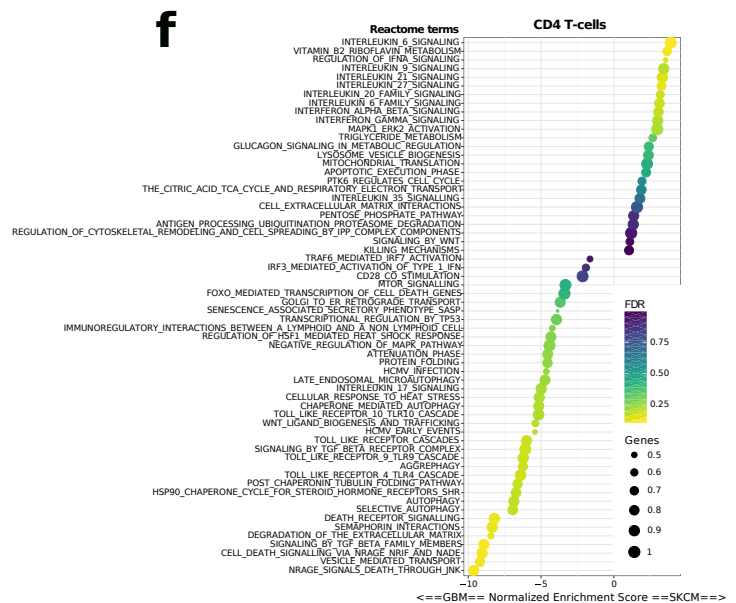
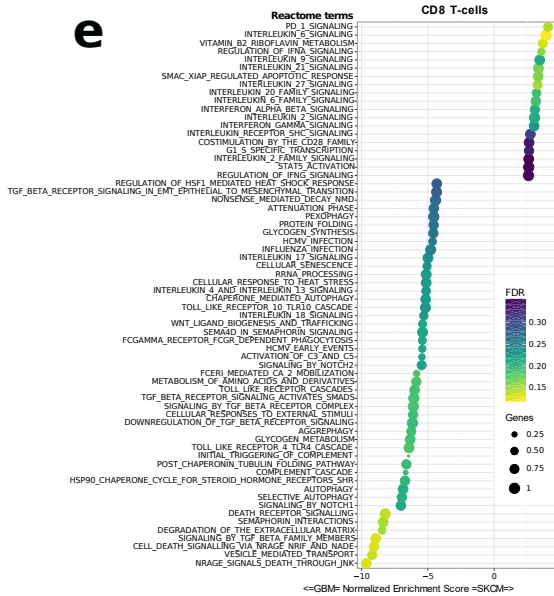
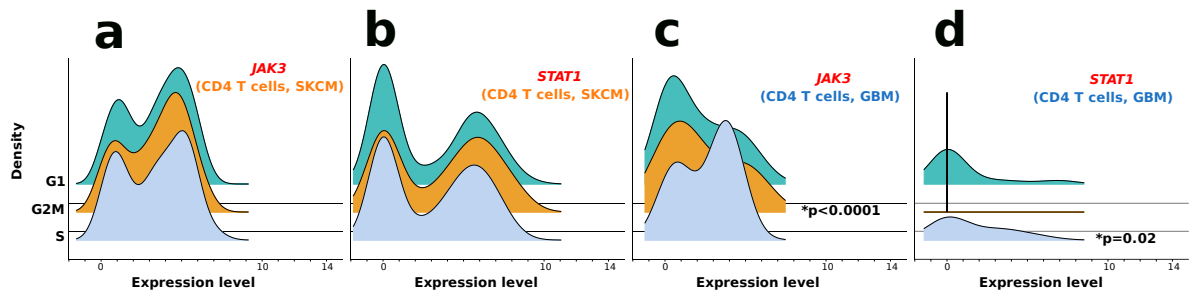


Supplementary Figure S6. (a-d) Dotplots highlighting differences in expression of indicated marker genes used for annotating the different $CD8^+$ (a,c) or $CD4^+$ (b,d) T-cell subpopulations (see **Supplementary Box. I**) as identified by the Leiden analysis in SKCM (a,b) or GBM (c,d) scRNASeq datasets.^{3,4} Solid black-borders indicate gene majorly used for annotating the subpopulation, based on available literature. **(e,f)** Density plots for a panel of genes-of-interest using the scRNASeq data analysed with STREAM for deeper appraisal of the effector-progenitor trajectory^{5,6} (e) or memory precursor-

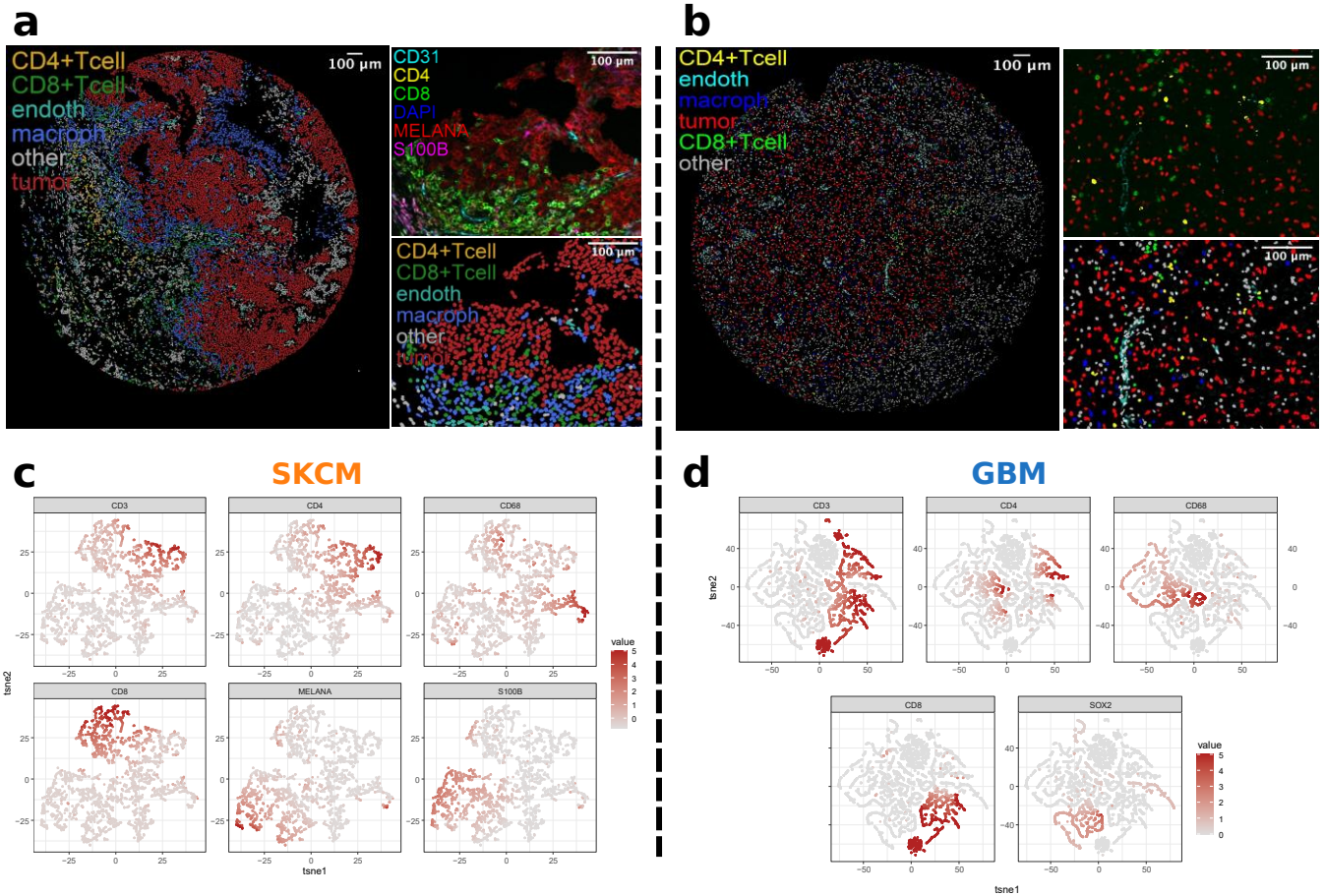
effector like trajectory⁷ with central/resident-memory and immunotolerant-phenotypes (f).⁸ The X-axis shows the inferred pseudotime, Y-axis represents the log₂-transformed TPM expression.



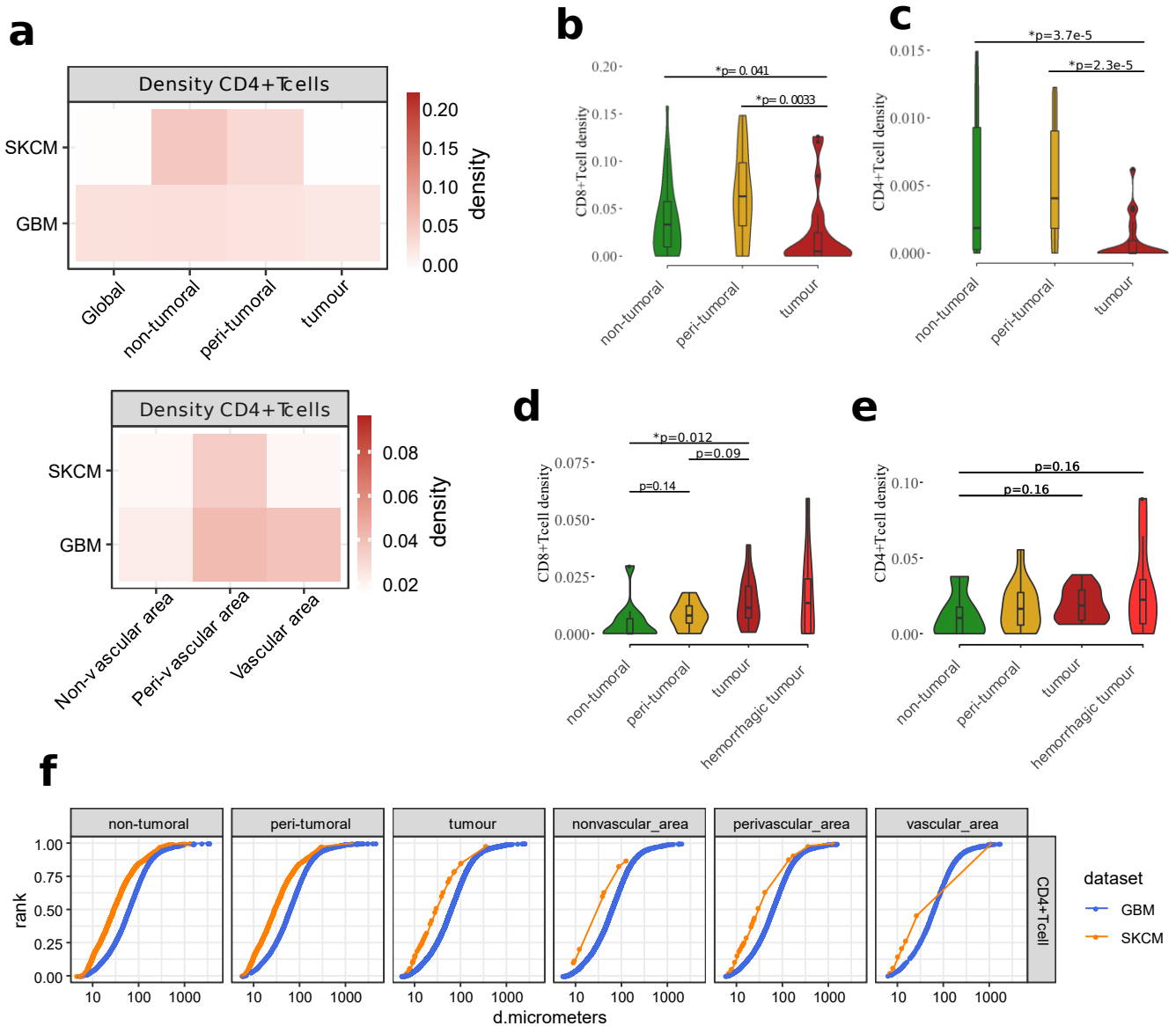
Supplementary Figure S7. Dotplots illustrating mean expression (colour) of the pairwise interaction and the probability (node size) of the interaction between ligand-receptor pairs (separated by “_”) between indicated single-cell types (separated by “|”) after running the CellPhoneDB pipeline.⁹ Herein, we depict the interactions between CD8⁺T cells::CD4⁺T cells, cancer cells::CD4⁺T cells or cancer cells::CD8⁺T cells, specific for SKCM-patients (a), specific for GBM-patients (c) or shared between SKCM and GBM patients (b,d) within the scRNASeq-dataset.^{3,4}



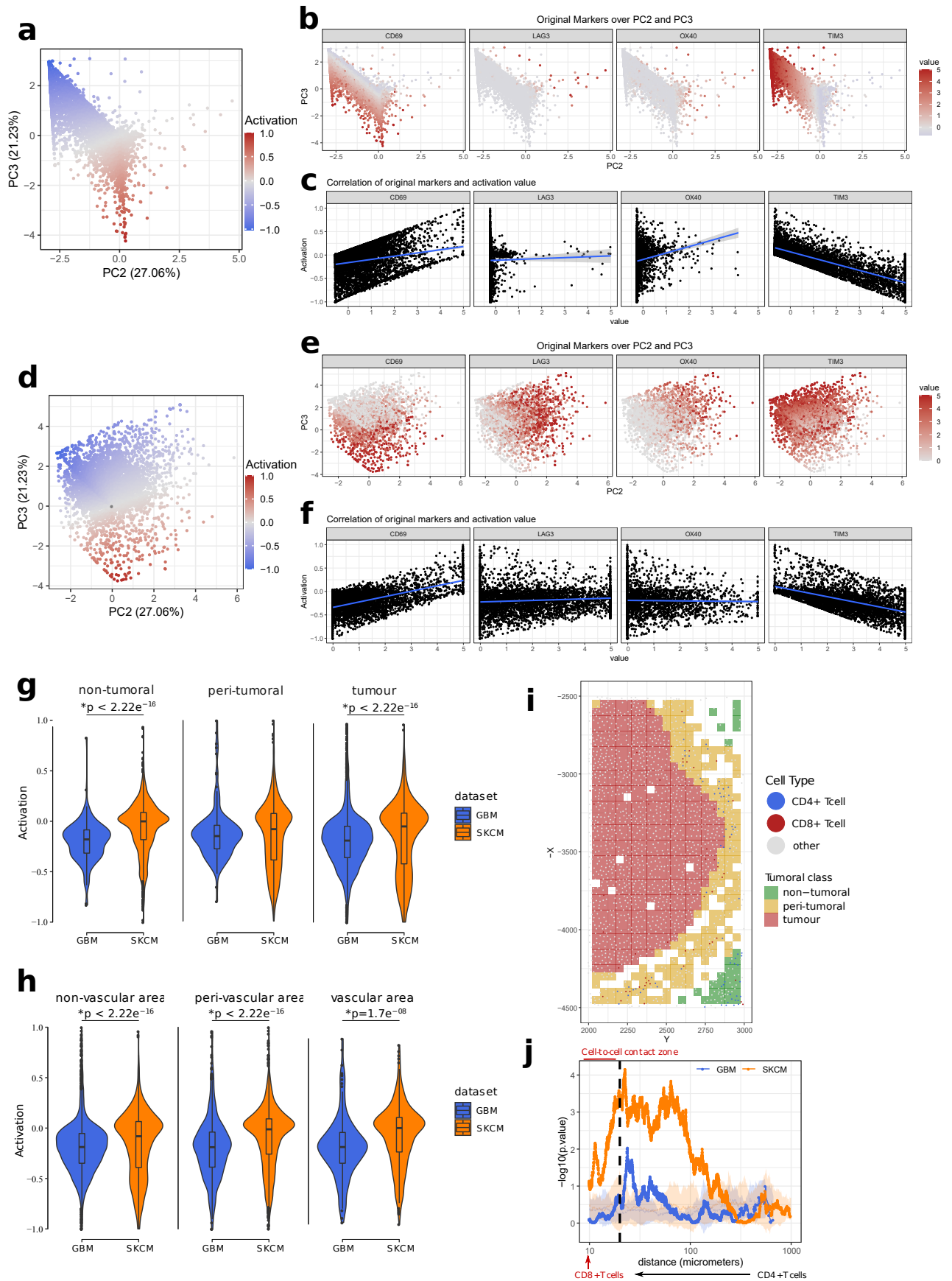
Supplementary Figure S8. (a-d) Ridge-plots illustrating the distribution of *JAK3*/*STAT1* expression in SKCM-CD4⁺T single-cells (a,b) and GBM-CD4⁺T single-cells (c,d) (statistics was estimated for SKCM vs. GBM comparison, for each gene per cell-cycle phase score; area-under-the-curve method combined with ANCOVA-analyses). (e,g) GSEA results for REACTOME pathways showing false-discovery rate (FDR) as colour intensity and normalized enrichment score on the X-axis between GBM and SKCM scRNASeq-data for CD8⁺T single-cells (e) or CD4⁺T single-cells (g). Dot size represents the number of major contributor genes in the pathway-enrichment, scaled between 0 to 1. (f) Volcano plot comparing GBM-CD4⁺T-cells to their SKCM counterparts, using scRNAseq data. P-values were Benjamini-Hochberg (BH)-adjusted. Statistical-significance threshold was * $p < 0.05$. For different gene-signatures, see **Supplementary-Table.2**.



Supplementary Figure S9. (a,b) Digital representations of the indicated tissue sections from Figure 5a/5e, with the indication of the various cell-types. Inserts with magnified regions are shown on the right of each image, containing the actual overlaid images (top) and the digital representation (bottom). **(c,d)** tSNE plots corresponding to Figure 5d/5h in which the expression of the indicated markers are highlighted for SKCM (n=10-samples across 10-patients) or GBM (n=11-samples across 8-patients) patient-derived tumours.

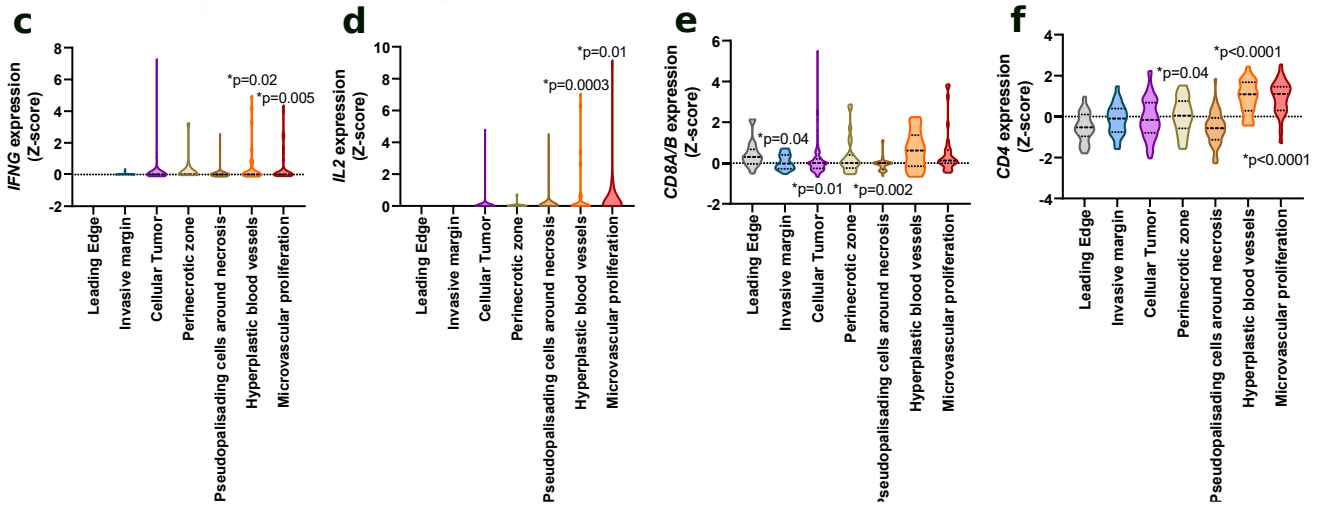
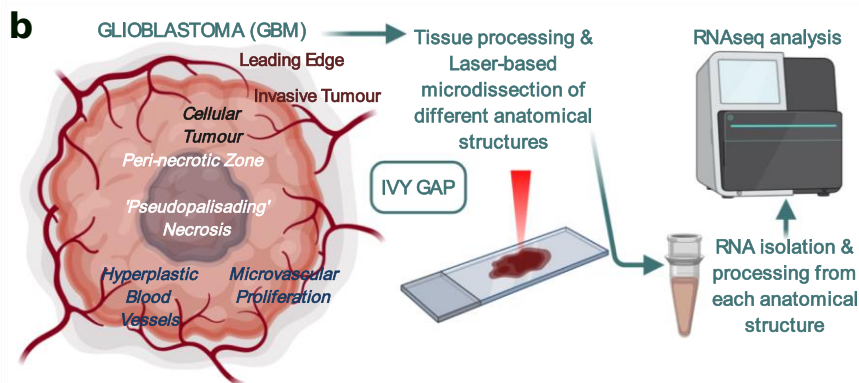
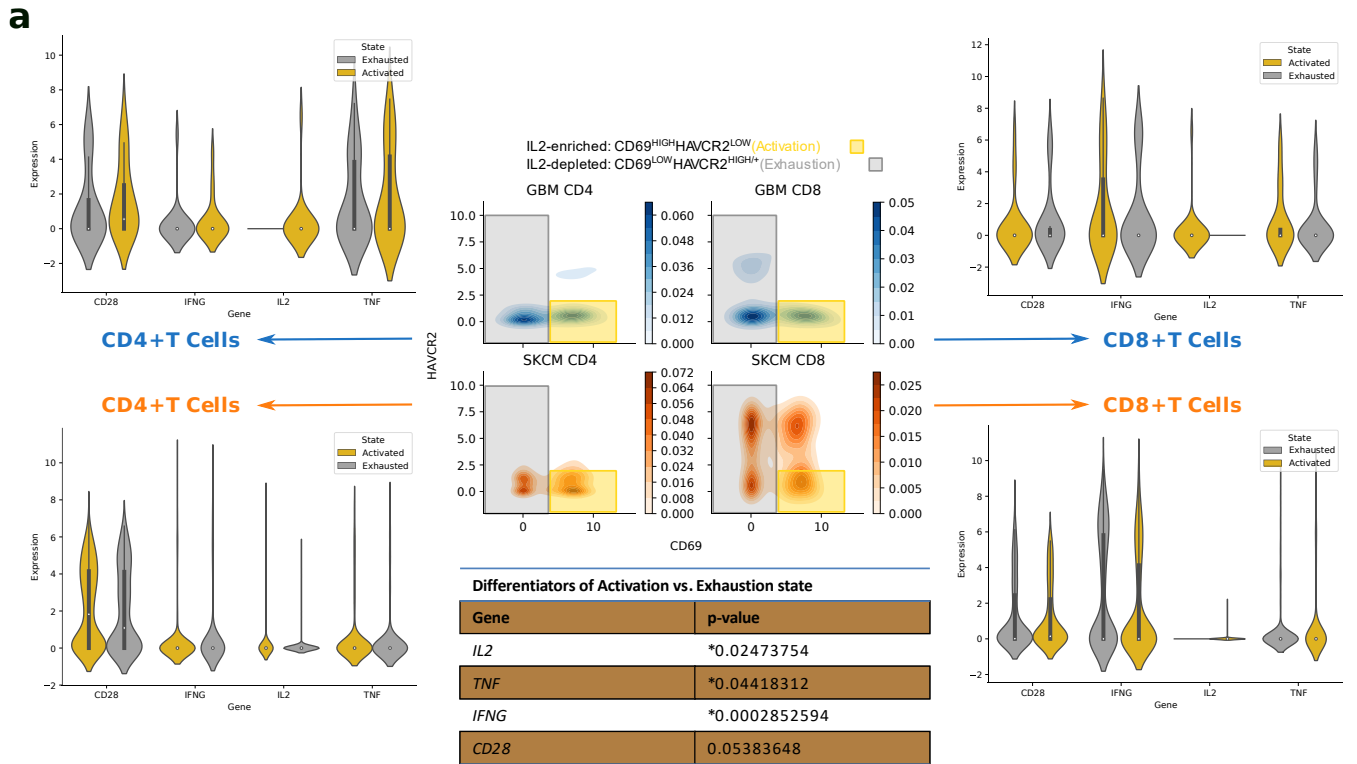


Supplementary Figure S10. (a-e) Density analysis of the CD4⁺T cell and CD8⁺T cell populations in GBM (n=11-samples across 8-patients) and SKCM (n=10-samples across 10-patients). Heat maps **(a)** show the relative distribution of CD4⁺T-cells across the indicated areas within each tumour type. **(b-e)** Violin plots indicate the SKCM-CD8⁺T cell **(b)**, SKCM-CD4⁺T cell **(c)**, GBM-CD8⁺T cell **(d)** or GBM-CD4⁺T cell **(e)** density distribution across the indicated areas within each tumour-type per patient (Mann-Whitney test with Holm-method for multiple-testing comparison; FDR-adjusted p-values are indicated). **(f)** Density analysis defining the relative proportion of CD4⁺T cells residing at the indicated distance (in micrometers/ μm) from the nearest CD8⁺T cell in SKCM or GBM tumours, across all analysed tissue-samples. Statistical-significance threshold was *p<0.05.



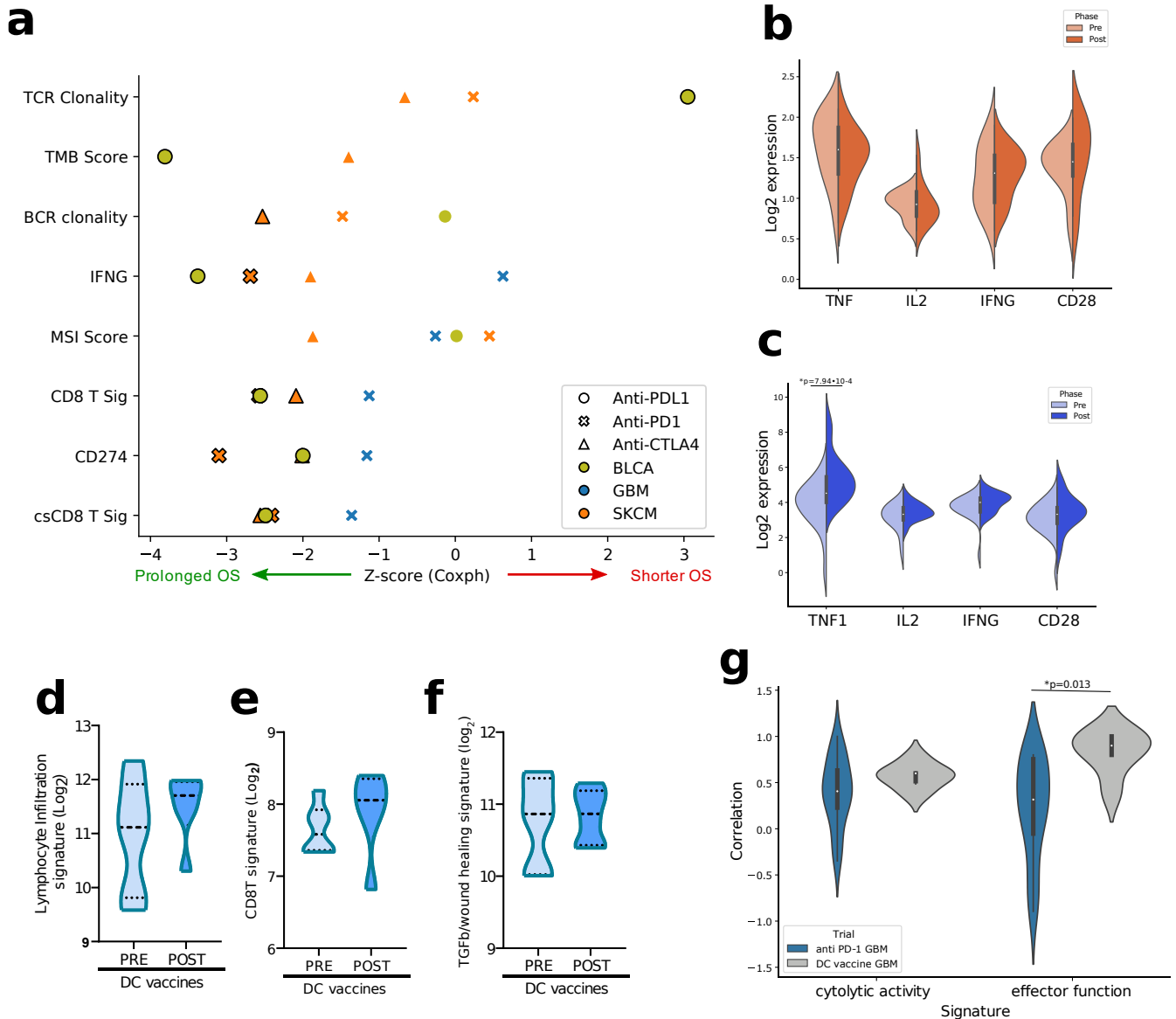
Supplementary Figure S11. (a,d) Dot plot representation showing the overall activation score distribution across all identified CD8⁺T cells in SKCM (n=10-samples across 10-patients) (a) and GBM (n=11-samples across 8-patients) (d). (b,c,e,f) Dot plot representation showing the break-up of the overall activation score across the different measured markers (b, e), and their correlation to the overall

activation score **(e,f)**. **(g,h)** Violin plots show the CD8⁺T cell activation levels across the indicated areas within each cancer-type (Mann-Whitney test with Holm-method for multiple-testing comparison; FDR-adjusted p-values are indicated). **(i)** Schematic, digital representation of an SKCM tumour sample with the CD4⁺ and CD8⁺ T cell populations, and their relative distribution across the different areas, as indicated. **(j)** Line plots showing the corresponding p-values to the median activation score of each CD8⁺T cell relative to the distance from the nearest CD4⁺T cell in each indicated cancer-type (one-tailed t-test; FDR adjusted p-values are indicated) (corresponding to **Figure 5I**).



Supplementary Figure S12. (a) $CD4^+/CD8^+$ single-cell level appraisal of the $CD69$ vs. $HAVCR2$ activation/exhaustion-model. $CD69^{LOW}HAVCR2^{HIGH/+}$ and $CD69^{HIGH}HAVCR2^{LOW}$ status was annotated as IL2-exhausted and IL2-activated based on “targeted” analyses of *IL2*, *IFNG*, *CD28* or *TNF* in these subpopulations (see, gates in the density plots). P-values were obtained with MAST to estimate

significance between activated and exhausted state. **(b)** Schematic overview of sampling, data procurement and analyses strategy of the IVY-GAP consortium's laser-assisted GBM tumour-tissue microdissection and anatomical sites-associated spatial transcriptomics.¹⁰ **(c-f)** Distribution of the z-score standardized expression of indicated genes based on the anatomical location in the GBM tumour micro-environment as annotated by the IVY-GAP consortium¹⁰ (Kruskal-Wallis ANOVA test with two-stage linear step-up procedure of Benjamini, Krieger and Yekutieli).



Supplementary Figure S13. (a) Clinical-trials involving pre-ICB (anti-PD1, anti-PDL1 or anti-CTLA4) treatment derived tumour-tissue from BLCA (n=298),¹¹ GBM (n=17)¹² or SKCM (anti-PD1 trial,¹³ n=41; anti-CTLA4 trial,¹⁴ n=42) patients were used for creating a comparison between the indicated biomarkers detected in pre-treatment tumour-tissue (Y-axis) and patient overall-survival (OS) estimated post-ICB treatment (OS represented as z-score in Coxph regression, X-axis) via the TIDE biomarker analyses platform.¹⁵ Biomarker symbols with bold-outline indicates *p<0.05. The arrows at the bottom indicate prolonged or shortened OS, post-ICB treatment. Herein, TCR is T cell receptor, BCR is B cell receptor, TMB is tumour-mutational burden, MSI is micro-satellite instability. Clinical-trials involving pre/post-ICB (anti-PD1) treatment derived tumour-tissue from SKCM (Pre, n=13; Post, n=11)¹⁶ or GBM (Pre, n=24; Post, n=25)¹⁷ patients were used for creating violin-plots for indicated genes within SKCM **(b)** or GBM **(c)** datasets (Welch's t-test). Clinical-trial involving pre/post-dendritic cell (DC)-vaccination derived tumour-tissue from GBM (Pre, n=6; Post, n=6) patients was used for creating: **(d-f)** violin-plots for indicated signature-levels (Mann-Whitney test); and **(g)** Violin-plots for correlations between pre- and post- treatment levels of cytolytic activity signature (*PRF1*, *GZMA*, *GZMB*, *GZMH*, *GZMK*, *TNFSF10*) and effector function signature (*IFNG*, *IL2*, *CD28*) in above anti-PD1 immunotherapy or DC-vaccination clinical trials in GBM patients. Statistical-significance threshold was *p<0.05.

References:

1. Thorsson, V. *et al.* The immune landscape of cancer. *Immunity* **48**, 812–830.e14 (2018).
2. Sun, D. *et al.* TISCH: a comprehensive web resource enabling interactive single-cell transcriptome visualization of tumor microenvironment. *Nucleic Acids Res.* (2020). doi:10.1093/nar/gkaa1020
3. Tirosh, I. *et al.* Dissecting the multicellular ecosystem of metastatic melanoma by single-cell RNA-seq. *Science* **352**, 189–196 (2016).
4. Neftel, C. *et al.* An integrative model of cellular states, plasticity, and genetics for glioblastoma. *Cell* **178**, 835–849.e21 (2019).
5. Kanev, K. *et al.* Proliferation-competent Tcf1+ CD8 T cells in dysfunctional populations are CD4 T cell help independent. *Proc. Natl. Acad. Sci. USA* **116**, 20070–20076 (2019).
6. Blank, C. U. *et al.* Defining “T cell exhaustion”. *Nat. Rev. Immunol.* **19**, 665–674 (2019).
7. Herndler-Brandstetter, D. *et al.* KLRG1+ Effector CD8+ T Cells Lose KLRG1, Differentiate into All Memory T Cell Lineages, and Convey Enhanced Protective Immunity. *Immunity* **48**, 716–729.e8 (2018).
8. Martin, M. D. & Badovinac, V. P. Defining memory CD8 T cell. *Front. Immunol.* **9**, 2692 (2018).
9. Efremova, M., Vento-Tormo, M., Teichmann, S. A. & Vento-Tormo, R. CellPhoneDB: inferring cell-cell communication from combined expression of multi-subunit ligand-receptor complexes. *Nat. Protoc.* **15**, 1484–1506 (2020).
10. Puchalski, R. B. *et al.* An anatomic transcriptional atlas of human glioblastoma. *Science* **360**, 660–663 (2018).
11. Mariathasan, S. *et al.* TGF β attenuates tumour response to PD-L1 blockade by contributing to exclusion of T cells. *Nature* **554**, 544–548 (2018).
12. Zhao, J. *et al.* Immune and genomic correlates of response to anti-PD-1 immunotherapy in glioblastoma. *Nat. Med.* **25**, 462–469 (2019).
13. Gide, T. N. *et al.* Distinct Immune Cell Populations Define Response to Anti-PD-1 Monotherapy and Anti-PD-1/Anti-CTLA-4 Combined Therapy. *Cancer Cell* **35**, 238–255.e6 (2019).
14. Van Allen, E. M. *et al.* Genomic correlates of response to CTLA-4 blockade in metastatic melanoma. *Science* **350**, 207–211 (2015).
15. Jiang, P. *et al.* Signatures of T cell dysfunction and exclusion predict cancer immunotherapy response. *Nat. Med.* **24**, 1550–1558 (2018).
16. Huang, A. C. *et al.* A single dose of neoadjuvant PD-1 blockade predicts clinical outcomes in resectable melanoma. *Nat. Med.* **25**, 454–461 (2019).
17. Schalper, K. A. *et al.* Neoadjuvant nivolumab modifies the tumor immune microenvironment in resectable glioblastoma. *Nat. Med.* **25**, 470–476 (2019).